Genomic Psychiatry

Genomic Press
Genomic Psychiatry
Advancing science from genes to society

OPEN

RESEARCH ARTICLE

Deciphering the molecular basis of accelerated biological aging in substance use disorder: Integrative transcriptomic analysis

Bruno Kluwe-Schiavon[1], Laura Stertz[1], Tatiana Barichello[1], Thomas D. Meyer[1], Gabriel R. Fries[1], and Consuelo Walss-Bass[1]

Substance use disorders (SUDs) contribute to early-onset age-related diseases and represent a major global health burden. Accelerated biological aging (AA) has been proposed as a key factor behind SUD-related morbidity and mortality. This study aimed to elucidate the molecular basis of AA in SUD by analyzing transcriptomic profiles in postmortem dorsolateral prefrontal cortex tissue from individuals with SUD, including alcohol (AUD), opioid (OUD), and stimulant use disorders (StUD). We examined brain tissue from 58 donors to assess differential aging patterns and AA across SUD using epigenetic clocks specifically designed for brain tissues (DNAmClock$_{Cortical}$, CerebralCortexClock$_{common}$, and PCBrainAge). Samples were then stratified into those with and without AA to perform differential expression analyses across groups and to identify biological pathways potentially related to AA. Analyses identified multiple differentially expressed genes linked to AA, revealing unique and overlapping biological pathways within SUD subtypes. Further, our analysis highlighted shared aging mechanisms across SUD subtypes, particularly mitochondrial signaling and metabolic processes. While insightful, these subtype-specific findings remain exploratory due to limited statistical power. Most biological pathways underlying AA in SUD appear to be subtype-specific, with distinct molecular signatures influenced by substance type. Given the cross-sectional design, causal interpretations are limited. Further research may support targeted interventions for aging-related risks in SUD populations.

Genomic Psychiatry (2025), 1–9; doi: https://doi.org/10.61373/gp025a.0029

Keywords: Epigenetic aging, postmortem brain, substance use disorders, transcriptome

Introduction

Substance use disorders (SUDs) lead to the early onset of age-related diseases and pose a critical global health challenge, ranking as the fifth cause of years lived with disability, the ninth cause of disability-adjusted life years, and the 15th cause of years of life lost due to premature mortality (1). SUDs are also associated with increased risks for chronic physical health conditions such as cardiovascular disease, cancer, chronic pain, and increased risk for long-term cognitive impairments (2, 3).

Biological aging is a process that describes the progressive deterioration of biological functions, in contrast to chronological aging, which represents the time since birth (4). Epigenetic clocks, such as Hannum, Horvath, PhenoAge, and GrimAge, which incorporate DNA methylation (DNAm) data from unique CpG sites across the genome into weighted linear equations to predict age and other health outcomes, are currently considered the most promising biomarkers of biological aging (5). Estimates of epigenetic accelerated aging (AA) are obtained by regressing the predicted epigenetic age against chronological age within a cohort, where positive values indicate faster-than-expected biological aging (6).

Emerging research has underscored the biological mechanisms underlying early-onset morbidity and premature mortality in SUD, with AA proposed as a potential driver of these adverse outcomes (7). This has been most consistently shown in alcohol use disorder (AUD), where patients exhibit biological ages that exceed their chronological ages and appear biologically older than controls in both brain and blood tissues when measured by the PhenoAge and Horvath clocks (8–12), and biological aging can be partly reversed with abstinence (10). Additionally, chronic heroin use has been associated with shorter DNAm-based telomere length (13). However, findings across SUDs such as stimulant use disorder (StUD) and opioid use disorder (OUD) are inconsistent. Assessments using first-generation epigenetic clocks such as Horvath and Hannum have shown no clear significant differences between these SUDs and control groups, and even counterintuitive negative biological aging has been reported (9, 12).

The absence of consistently higher AA in some SUDs does not negate its relevance; rather, the findings from current studies imply that adverse aging outcomes in SUD may be driven by distinct biological processes and that the degree of AA may vary based on substance-specific effects and the type of epigenetic clock used for assessment. In regards to the latter, although previous studies, including our own, have shown that epigenetic clocks designed for use in peripheral blood may serve as good estimators of brain aging (8), the extent of AA in SUD in the brain has not previously been comprehensively explored using epigenetic clocks specifically designed for brain tissues. In this study, we aimed to identify substance-specific transcriptomic profiles of AA in the dorsolateral prefrontal cortex (DLPFC, Brodmann area [BA] 9), a key region involved in cognitive processes relevant to SUD, such as executive functions, decision-making, behavioral and cognitive inhibition, working memory, and craving (14). Specifically, we hypothesized that distinct drug-specific biological pathways would influence AA in SUD, potentially explaining the variability in aging outcomes observed in these disorders.

In this study, we explored the relationship between SUD and epigenetic markers of AA, focusing on AUD, OUD, and StUD. By concentrating on specific SUDs, we aimed to clarify substance-specific aging patterns and minimize confounding effects that could arise from broader case-control comparisons. Our objectives were: (i) to identify differentially expressed genes (DEGs) associated with AA in individuals with SUD and (ii) to explore overlaps in enriched biological pathways and mechanisms across different SUD subtypes (AUD, OUD, and StUD) related to AA.

Results

Participant demographic, clinical, and biological characteristics are summarized in Table 1 and Supplementary Table S2. The identified AA+ and

[1]Faillace Department of Psychiatry and Behavioral Sciences, McGovern Medical School, University of Texas Health Science Center at Houston (UTHealth), Houston, TX 77054
Corresponding Authors: Gabriel R. Fries, University of Texas Health Science Center at Houston, 1941 East Rd, Houston, TX 77054, USA. Phone: 713-486-2629. E-mail: Gabriel.R.Fries@uth.tmc.edu; and Consuelo Walss-Bass Phone: 713-486-2718. E-mail: Consuelo.walssbass@uth.tmc.edu
Received: 26 February 2025. Revised: 8 April 2025 and 10 April 2025. Accepted: 11 April 2025.
Published online: 29 April 2025.

Table 1. Sample characteristics and group comparisons

	Overall	AA−	AA+	Statistics	*p*-value	Effect size
Sample size, freq.	58	30	28			
Age, mean (SD)	45.84(14.49)	44.33(16.54)	47.46(12.01)	t[52.89] = −0.83	0.411	0.113
Sex, freq. (%)	15(25.9)	6(20.0)	9(32.1)	Ï‡Â^2[1] = 0.57	0.45	0.139
Smoking index, mean (SD)	0.82(0.05)	0.83(0.06)	0.81(0.05)	t[56] = 1	0.32	0.133
Race: White, freq. (%)	35(60.3)	16(53.3)	19(67.9)	Ï‡Â^2[1] = 0.74	0.389	0.148
Race: Black, freq. (%)	17(29.3)	9(30.0)	8(28.6)	Ï‡Â^2[1] = 0	0.999	0.016
Race: Hispanic, freq. (%)	6(10.3)	5(16.7)	1(3.6)	Ï‡Â^2[1] = 1.45	0.228	0.215
AUD, freq. (%)	13(22.4)	6(20.0)	7(25.0)	Ï‡Â^2[1] = 0.02	0.888	0.06
OUD, freq. (%)	16(27.6)	10(33.3)	6(21.4)	Ï‡Â^2[1] = 0.52	0.472	0.133
StUD, freq. (%)	10(17.2)	4(13.3)	6(21.4)	Ï‡Â^2[1] = 0.22	0.64	0.107
AUD and OUD, freq. (%)	6(10.3)	4(13.3)	2(7.1)	Ï‡Â^2[1] = 0.12	0.732	0.102
AUD and StUD, freq. (%)	5(8.6)	3(10.0)	2(7.1)	Ï‡Â^2[1] = 0	0.999	0.051
OUD and StUD, freq. (%)	3(5.2)	1(3.3)	2(7.1)	Ï‡Â^2[1] = 0	0.951	0.086
Polysubstance use disorder, freq. (%)	5(8.6)	2(6.7)	3(10.7)	Ï‡Â^2[1] = 0.01	0.936	0.072
Cause of death: Cardiovascular/Chronic conditions, freq. (%)	22(37.9)	11(36.7)	11(39.3)	Ï‡Â^2[1] = 0	0.999	0.027
Cause of death: Overdose, freq. (%)	34(58.6)	19(63.3)	15(53.6)	Ï‡Â^2[1] = 0.24	0.626	0.099
Cause of death: Other, freq. (%)	2(3.4)	–	2(7.1)	Ï‡Â^2[1] = 0.59	0.441	0.196
PCBrainAgeClockAcc, mean (SD)	0.05(3.95)	−1.87(3.79)	2.11(3.00)	t[54.59] = −4.44	0.999	0.515
DNACorticalClockAcc, mean (SD)	−0.30(3.44)	−2.42(2.65)	1.97(2.64)	t[55.74] = −6.32	0.999	0.646
CerebralCortexClockCommonAcc, mean (SD)	−0.49(3.34)	−2.65(2.18)	1.84(2.76)	t[51.38] = −6.83	0.999	0.69
PCHorvath1Acc, mean (SD)	0.00(3.79)	−0.92(4.03)	0.98(3.30)	t[55.12] = −1.97	0.054	0.256
PCHorvath2Acc, mean (SD)	0.00(2.47)	−0.62(2.60)	0.66(2.18)	t[55.37] = −2.03	0.047	0.263
PCHannumAcc, mean (SD)	0.00(1.47)	−0.17(1.53)	0.19(1.41)	t[56] = −0.94	0.353	0.124
PCPhenoAgeAcc, mean (SD)	0.00(1.73)	−0.18(1.83)	0.20(1.63)	t[55.89] = −0.84	0.405	0.112
PCGrimAgeAcc, mean (SD)	0.00(1.12)	0.12(1.04)	−0.13(1.21)	t[53.57] = 0.84	0.403	0.114
Batch, freq. (%)	20(34.5)	9(30.0)	11(39.3)	Ï‡Â^2[1] = 0.22	0.64	0.098
PMIhrs, freq. (%)	26.23(7.64)	27.66(8.20)	24.69(6.80)	t[55.25] = 1.51	0.138	0.199
RIN Novogene, freq. (%)	7.18(0.96)	7.03(0.99)	7.35(0.91)	t[55.98] = −1.28	0.206	0.169
pH, freq. (%)	6.54(0.28)	6.55(0.29)	6.53(0.28)	t[55.94] = 0.21	0.831	0.029
dtangle: Astrocytes, freq. (%)	0.32(0.15)	0.34(0.15)	0.30(0.16)	t[55.04] = 1.02	0.314	0.136
dtangle: Endothelia, freq. (%)	0.09(0.02)	0.08(0.02)	0.09(0.02)	t[53.01] = −0.9	0.372	0.123
dtangle: Microglia, freq. (%)	0.05(0.02)	0.05(0.01)	0.05(0.02)	t[46.69] = −0.42	0.676	0.062
dtangle: Neurons, freq. (%)	0.40(0.13)	0.39(0.12)	0.42(0.13)	t[54.76] = −0.96	0.341	0.129
dtangle: Oligodendrocytes, freq. (%)	0.07(0.03)	0.06(0.03)	0.07(0.04)	t[48.75] = −1.06	0.292	0.151
dtangle: OPCs, freq. (%)	0.07(0.02)	0.07(0.01)	0.07(0.02)	t[51.77] = 1.27	0.211	0.173

The Student *t* test was used to compare the ages of the different groups, with the effect size reported as an *r* statistic. For *r*, values of 0.1, 0.3, and 0.5 denote small, moderate, and large effects, respectively. The chi-square test was employed for categorical variables, with effect sizes reported using Cramér's V. For Cramér's V, values of 0.1, 0.3, and 0.5 indicate small, moderate, and large effects, respectively.

AA+ groups were comparable across variables such as chronological age, sex distribution, and racial composition. Supplementary Figure S2 shows the overlap of AA between SUD types.

Differential Expression and Pathway Enrichment Analyses

DEG analyses between the AA+ and AA− groups were carried out within all SUD (AA+, $n = 28$; AA−, $n = 30$) and then individually within each SUD subtype: AUD (AA+, $n = 7$; AA−, $n = 6$), OUD (AA+, $n = 6$; AA−, $n = 10$), and StUD (AA+, $n = 6$; AA−, $n = 4$). We identified 11 DEGs in the combined SUD analysis (Supplementary Table S3). At the same time, exploratory analyses in the SUD subgroups revealed 463 DEGs in primary AUD (Figure 1A; Supplementary Table S4), 58 in primary OUD (Figure 1B; Supplementary Table S5), and 51 in StUD (Figure 1C; Supplementary Table S6). Notably, only a few DEGs were shared across all SUD subgroups (Figure 1D). Gene Ontology (GO) biological process (BP) pathway analyses revealed significant enrichment in 85 pathways in AUD (Supplementary Table S7), 9 in OUD (Supplementary Table S8), and 17 in StUD (Supplementary Table S9). The top 10 pathways from the GO BP enrichment analyses conducted for all SUD subgroups in DEG are shown in Table 2. Though insightful, these subtype-specific findings remain exploratory due to limited statistical power.

SUD Subgroups Overlaps

DEG Overlaps Between AUD and OUD. Among SUD subgroups, a larger overlap in the DEGs between AA+ when compared with AA− was found for the AUD and the OUD groups (Table 3). Remarkably, most of the genes were downregulated in AA+ when compared with AA− within OUD but upregulated within AUD (*TRIOBP, TNS2, NIBAN2,* and *SOX17*), while the others had the exact opposite pattern, being upregulated in AA+ when compared with AA− within the OUD but downregulated within AUD (*RAB3C, PGM2L1,* and *ROBO2*).

DEG Overlaps Between AUD and StUD. Five DEGs were found to overlap among the AUD and StUD groups: *EDN1, HBA2, HBA1, AQP1,* and *HBB* (Table 3). Within the AUD group, all these genes were upregulated in AA+ when compared with AA−. However, within the StUD group, only *AQP1* was upregulated, while *EDN1, HBA2, HBA1,* and *HBB* were downregulated. These contrasting patterns suggest different biological responses in these groups concerning aging in AUD and StUD.

DEG Overlaps Between OUD and StUD. Two DEGs were identified as overlapping among the OUD and StUD groups (Table 3): *TTYH2* and *TMEM63A*.

https://doi.org/10.61373/gp025a.0029

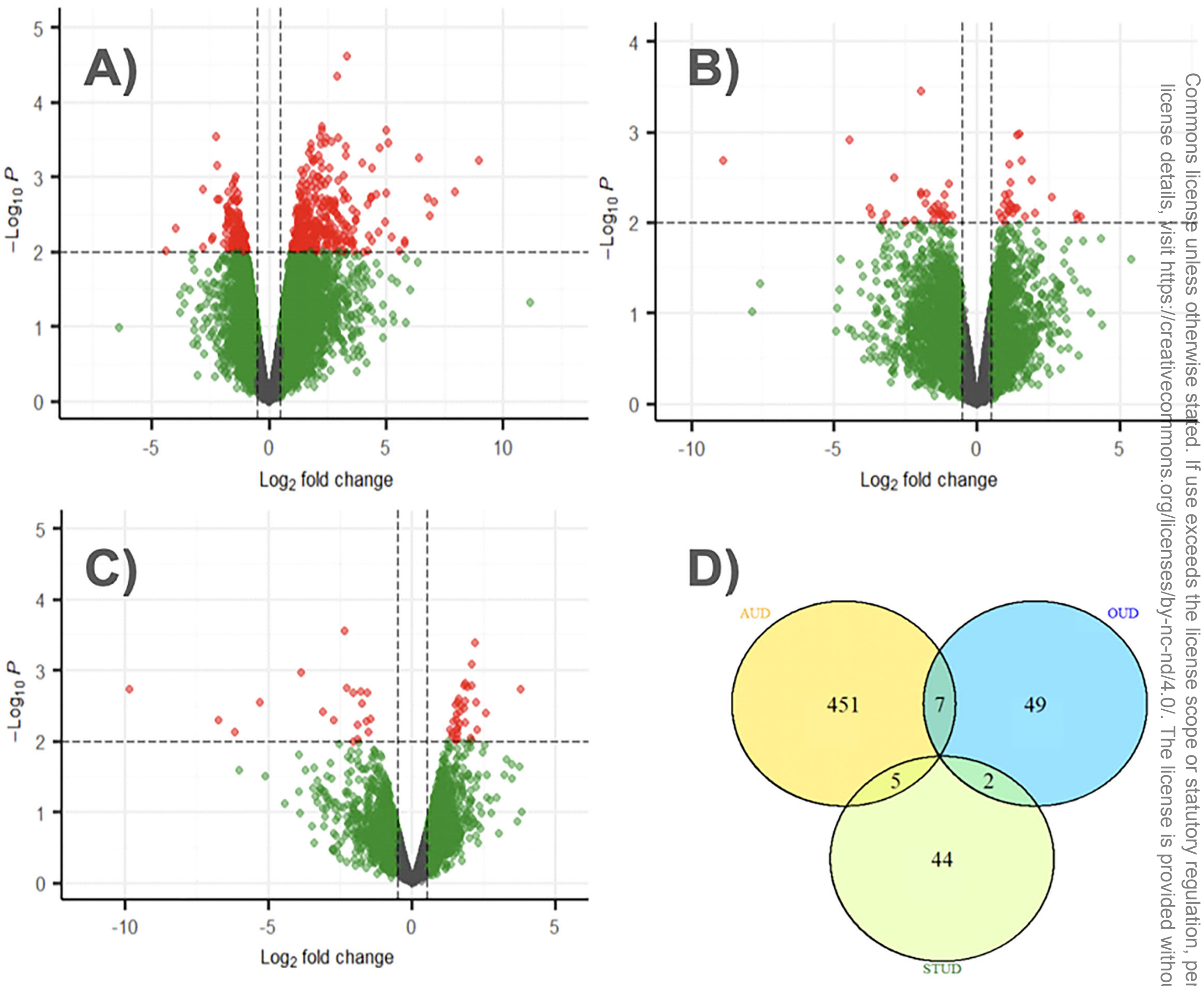

Figure 1. Differential expression in DLPFC of SUD subjects with accelerated biological aging compared to those without. Volcano plots show differences between accelerated aging positive (AA+) and accelerated aging negative (AA−) in (A) AUD(AA+, $n = 7$; AA−, $n = 6$); (B) OUD (AA+, $n = 6$; AA−, $n = 10$); and (C) StUD (AA+, $n = 6$; AA−, $n = 4$). The Venn Diagram (D) shows the overlaps between the differentially expressed genes identified. As we can see, five genes were differentially expressed when comparing AA+ and AA− in both AUD and StUD; seven genes were differentially expressed when comparing AA+ and AA− in both AUD and OUD; and two genes were differentially expressed when comparing AA+ and AA− in both OUD and StUD.

Both genes were downregulated in AA+ when compared with AA− in OUD, while in the StUD group, they were upregulated in AA+.

Molecular Mechanisms Linking Differential Gene Expression Across SUDs

Figure 2 illustrates a hypothetical molecular framework integrating DEGs from enriched pathways identified in AUD, StUD, and OUD (Table 2), highlighting key biological pathways involved in neuroinflammation, mitochondrial dysfunction, and oxidative stress as potential mechanisms underlying AA in SUD. The diagram highlights interactions among transcription factors, inflammatory mediators, and mitochondrial regulators, suggesting distinct but converging pathways contributing to cellular stress, mitochondria function, and neuroinflammation across SUD subtypes.

Discussion

To our knowledge, this is the first study investigating brain AA in SUDs using epigenetic clocks specifically designed for brain tissues ($DNAmClock_{Cortical}$, $CerebralCortexClock_{common}$, and PCBrainAge). Notably, we found that despite the high correlation between the clocks, the contribution of the variables observed in our principal component analyses (PCA), along with the innovative dichotomous classification of our sample, emphasized that the three brain-specific epigenetic clocks have distinct characteristics and do not necessarily converge when classifying individuals based on their AA. Hence, our findings align with the idea that each clock might capture unique aspects of aging. As we noted in the Method section, while this PC1-based dichotomization facilitates downstream comparisons, it represents a simplification of what is likely a continuous biological process. This classification should, therefore, be interpreted as a pragmatic, exploratory strategy to investigate broad molecular differences associated with higher versus lower levels of epigenetic aging in the brain.

Overall, the differential gene expression and pathway analysis findings suggest that AA in SUD is not a uniform process but that distinct biological mechanisms contribute to aging, depending on the type of substance involved. The most robust differences between AA+ and AA− were observed in the AUD group, which aligns with previous research showing an effect of AUD on AA (9, 12). Enrichment analyses suggest that AA is related to protein phosphorylation, signal transduction, and the positive regulation of protein localization to the plasma membrane. Protein phosphorylation and signal transduction are essential processes often altered in both normal aging and disease progression (15, 16). Furthermore, the finding of enrichment of glutamatergic synapse pathways aligns with studies suggesting a critical role of glutamate in both aging and

Table 2. Top 10 GO BP pathways identified when comparing AA+ and AA− in SUD groups

Term	Genes	Fold enrichment
Alcohol use disorder		
Positive regulation of integrin-mediated signaling pathway	LAMB2, EMP2, LIMS2	9.699*
Cellular response to zinc ion	MT2A, MT1M, MT1X, MT3, MT1E	9.429**
Intracellular zinc ion homeostasis	MT2A, SLC30A9, MT1M, MT1X, MT3, SLC39A14, MT1E	9.052***
Negative regulation of endocytosis	LGALS3, RUBCN, SYT11	9.052*
Positive regulation of G protein-coupled receptor signaling pathway	GPER1, TMOD2, SLC39A14	9.052*
Removal of superoxide radicals	NOS3, MT3, SOD3	8.487*
Regulation of store-operated calcium entry	CRACR2B, HOMER1, SLC8B1	8.487*
Positive regulation of leukocyte migration	MADCAM1, ZP3, VEGFA	8.487*
Negative regulation of viral genome replication	IFITM3, SRPK2, IFITM2, RSAD2, MX1, EIF2AK2, IFIT1	6.888***
Platelet-derived growth factor receptor signaling pathway	NR4A3, TXNIP, PTPRJ, CSPG4, PLAT	6.858**
Opioid use disorder		
Central nervous system development	ROBO2, CITED2, ZIC3, ID3	9.997**
Outer ear morphogenesis	EYA1, ZIC3	78.31***
Metanephros development	ROBO2, SOX17, EYA1, ID3	46.986***
Positive regulation of execution phase of apoptosis	TP53BP2, HTR2A	46.986***
Positive regulation of gene expression	IL32, SOX17, CSF1, CITED2, HDAC1, ID3	4.154*
Left/right axis specification	CITED2, ZIC3	3.915*
Positive regulation of DNA-templated transcription	NIBAN2, SOX17, CITED2, HDAC1, ZIC3, TRIM21, NPAS3	3.46*
Outflow tract morphogenesis	SOX17, EYA1, CITED2	19.947*
Heart looping	SOX17, CITED2, ZIC3	14.89*
Stimulant use disorder		
Central nervous system development	UGTB, RELN, MOG	8.933*
Oxygen transport	HBB, HBA2, HBA1	78.726***
Positive regulation of fibroblast migration	THBS1, AQP1	64.596**
Semaphorin-plexin signaling pathway involved in axon guidance	EDN1, PLXNB3	55.983*
Cell adhesion	CLDN11, MAG, RELN, MOG, PCDHGB2, CCN1, THBS1	5.685*
Transport	ALB, AFP	46.652*
Response to hydrogen peroxide	HBB, HBA2, HPR, HBA1	45.392**
Response to muscle stretch	EDN1, NPPA	44.197*
Hydrogen peroxide catabolic process	HBB, HBA2, HBA1	43.435**
Nitric oxide transport	EDN1, HBB, HBA2, HBA1, AQP1	419.872***

$^{*}< .05$, $^{**}< .01$, $^{***}<.001$.

neurodegenerative processes and highlights the role of glutamatergic signaling in maintaining synaptic plasticity and cognitive function (17). Regarding OUD, we identified transcriptional regulation, neurodevelopment, and immune-inflammatory processes as key drivers of AA. We also found that positive regulation of DNA-templated transcription, which includes the genes *NIBAN2*, *SOX17*, and *HDAC1*, contributes to transcriptional age-related alterations in OUD. This finding aligns with previous studies on transcriptional dysregulation in aging and highlights the role of histone methylation in this process (18). Concerning StUD, our findings emphasize the role of oxidative stress, hypoxia responses, and cell adhesion pathways. As supported by (18), oxidative stress has an important impact on aging, particularly in the development of chronic diseases like cardiovascular disorders (18).

Table 3. Overview of comparisons between accelerated aging groups (AA+ vs. AA−) and overlaps between groups

	DEG ($p < .01$, FC <> .5)	GO:BP ($p < .05$)
SUD	11	6
AUD	463	85
OUD	58	9
StUD	51	17
AUD ∩ OUD	7	2
AUD ∩ StUD	5	6
OUD ∩ StUD	2	1
AUD ∩ OUD ∩ StUD	0	0

This table provides an overview of all comparisons between individuals with accelerated biological aging (AA+) and those without (AA−), including overlaps between SUD groups. Differential gene expression (DEG) analysis was performed for each group. The top rows summarize the number of DEGs and enriched pathways identified in the AA+ versus AA− analyses for each SUD group. The bottom rows present overlaps between SUD subgroups (AUD and OUD; AUD and StUD; OUD and StUD; AUD and OUD and StUD), including DEGs and enriched pathways shared across comparisons.

Our integrative mechanistic analysis identified neuroinflammation, oxidative stress, and mitochondrial dysfunction to be implicated in AA across all SUD subtypes. Mitochondria function is central to maintaining cellular energy homeostasis and regulating oxidative stress responses (15). DEGs such as *NOS3, TXNIP, HTR2A, CSF1, HDAC1, EDN1, THBS1,* and *RELN* are directly implicated in mitochondrial dysfunction and ROS production and can activate the assembly of *NLRP3* through different mechanisms (19–22). The cerebral expression of *NOS3* has been associated with molecular abnormalities related to neurodegeneration, including oxidative stress and mitochondrial dysfunction (19). *TXNIP* overexpression significantly increases mitochondrial complex II activity and promotes the expression of *SDHA*, a subunit of complex II, which is a significant site for reactive oxygen species (ROS) generation (20). ROS production by CSF-1 is crucial for macrophage functions such as pathogen killing, cell signaling, and inflammatory responses (21). *THBS1* activates latent transforming growth factor-beta 1 (TGF-β1), a crucial cytokine involved in inflammation, wound healing, and immune responses, and *THBS1* stimulates the production of ROS through its interaction with *CD47* (23, 24). *HDAC1* can both promote and suppress

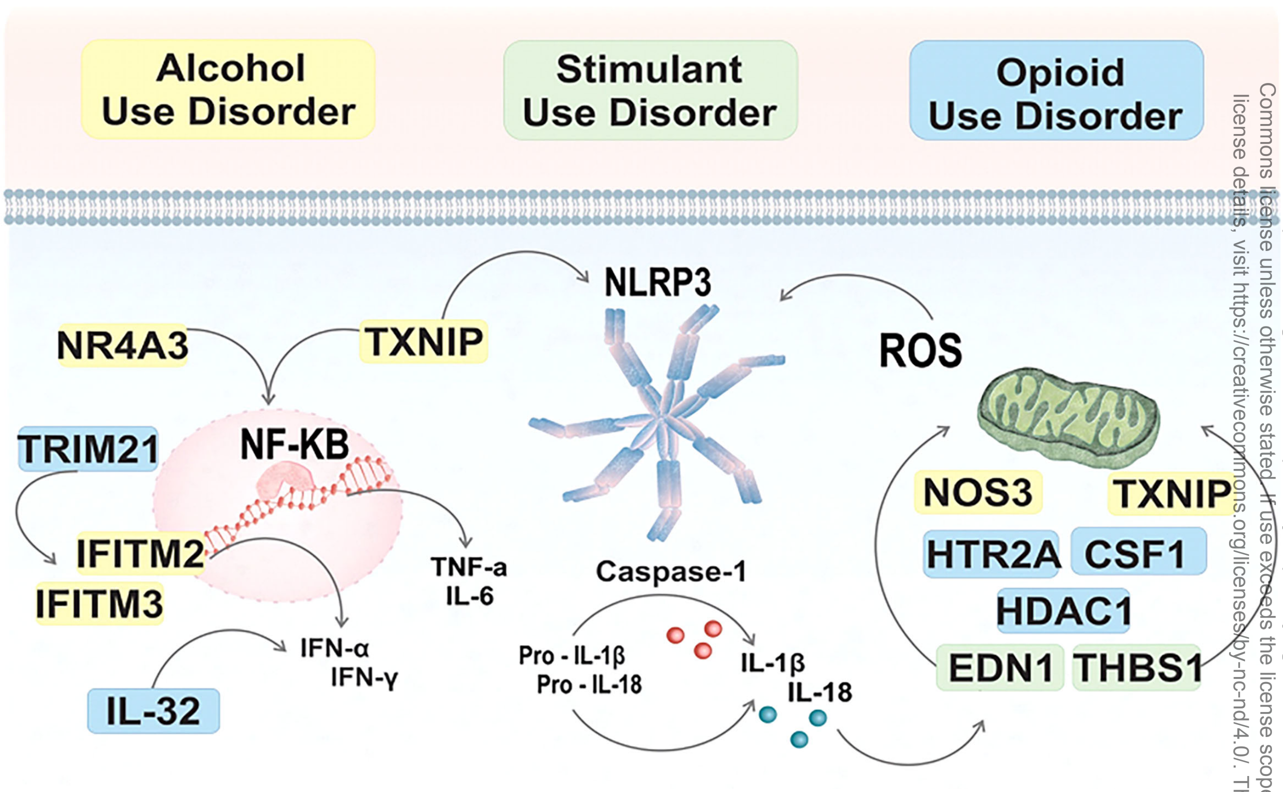

Figure 2. Inflammation and mitochondrial function as mechanisms in AA across SUDs. This figure presents a proposed model linking genes associated with neuroinflammatory and oxidative stress-related pathways across three major SUDs when comparing accelerated aging positive (AA+) and accelerated aging negative (AA−). Genes that are shown in yellow were observed in aging-related pathways within AUD, while the ones in green were observed in aging-related pathways within StUD, and the ones in blue within OUD. The nuclear factor-kappa B (NF-κB) pathway is activated by genes such as *NR4A3*, *TRIM21*, *IFITM2*, *IFITM3*, and *IL-32*, which are involved in inflammatory signaling and immune regulation and might contribute to the production of proinflammatory cytokines (e.g., IFN-α, IFN-γ, TNF-α, IL-6) that may exacerbate neuronal damage. Furthermore, the *TXNIP* and *HDAC1* contribute to inflammasome activation, leading to increased Caspase-1 activity and the subsequent maturation of IL-1β and IL-18, promoting neuroinflammatory responses. Future studies might investigate the role of NLRP3 as a central component in stimulant-induced neuroinflammation in this mechanism. Finally, the upregulation of NOS3, TXNIP, CSF1, HTR2A, HDAC1, EDN1, THBS1, and RELN is linked to vascular dysfunction, cellular stress, and neurodegeneration, might contribute to mitochondrial dysfunction and oxidative stress (ROS).

inflammatory signaling depending on environmental stimuli, which may also influence ROS production (25). *SOX17*, in particular, has been implicated in mitochondrial homeostasis and metabolic regulation, as it influences ATP production, oxidative stress balance, and mitochondrial biogenesis, which are essential for cellular energy metabolism and differentiation (26, 27). Its role in regulating transcription factors such as *HNF1B* and *FOXA2* also highlights its broader impact on mitochondrial function and metabolic adaptation (26).

It is worth mentioning that opposite patterns of regulation were observed in overlapping DEGs for SUD subtypes. For instance, the differential expression of *SOX17* in AUD and OUD may reflect distinct substance-specific effects on cellular stress responses and mitochondrial function in AA+ individuals. In AUD, *SOX17* appears to be upregulated, potentially indicating a compensatory mitochondrial response to alcohol-induced oxidative stress, excitotoxicity, and inflammation (28, 29). In contrast, *SOX17* is downregulated in OUD, which may reflect a blunted or exhausted mitochondrial stress response. As mentioned before, opioids have been shown to impair mitochondrial respiration, increase ROS production, and dysregulate energy metabolism—factors that could lead to suppressed transcriptional regulators like *SOX17*. Another example is NIBAN2, which is upregulated when cells are under stress. We found that *NIBAN2* is upregulated in AUD and downregulated in OUD. In AUD, alcohol-induced oxidative stress may drive the upregulation of *NIBAN2* as a compensatory response to mitigate damage. In contrast, OUD's impact on mitochondrial dysfunction and ROS production may suppress transcriptional responses, leading to the downregulation of *NIBAN2*.

Several limitations of the present study should be acknowledged. The relatively small sample size limits the generalizability of the findings, particularly when subdividing the SUD group into specific subtypes. It is important to emphasize that the SUD subgroups were strictly based on the primary diagnosis determined by the consensus diagnosis process. We excluded participants meeting criteria for any additional SUD diagnoses, as determined from the psychological autopsy. Future studies with larger sample sizes are required to confirm our findings and to further elucidate the mechanisms of AA in different SUDs. The cross-sectional design of this study inherently limits our ability to conclude causality or the temporal progression of AA in individuals with SUD. While we identified associations between molecular profiles and AA status, we cannot determine whether these epigenetic and transcriptomic signatures reflect causal mechanisms, compensatory adaptations, or consequences of long-term substance use. Longitudinal studies that track individuals over time—ideally from active substance use through abstinence or relapse—are essential to disentangle the directionality of these associations and to better understand how biological aging evolves in the context of substance use and related risk factors. Additionally, while our models accounted for several biological and technical covariates, including RNA integrity, tissue pH, smoking index, batch, and estimated cell-type proportions, we acknowledge the likelihood of residual confounding. This limitation is inherent to postmortem studies, where comprehensive individual-level data are often difficult to obtain. Although we conducted detailed psychological autopsy interviews with the donors' next-of-kin and used a rigorous diagnostic consensus process to

https://doi.org/10.61373/gp025a.0029

determine primary SUD diagnoses, information regarding psychiatric comorbidities, psychotropic medication use, or other medical conditions may be incomplete or inaccurate. These unmeasured factors could influence gene expression and epigenetic profiles and may partially confound our findings. Future studies leveraging larger cohorts and incorporating more detailed clinical records are needed to disentangle these complex relationships. Finally, significant DEGs were identified based on a nominal *p*-value threshold of 0.01 and a fold-change cutoff of 0.5. Notably, no genes survived FDR correction, and thus, all results should be interpreted as exploratory.

In conclusion, this study provides valuable insights into the molecular mechanisms underlying AA in SUD. By identifying genes and enriching biological pathways across various SUDs, we underscore the complexity of substance-induced accelerated epigenetic aging in the brain. Some shared mechanisms of AA between SUD subtypes were noted. Particularly, genes involved in metabolic regulation and mitochondrial function were identified across all disorders. Vascular and oxygen transport system alterations were common in AUD and StUD; cellular signaling, neurodevelopment, and metabolic processes in AUD and OUD; and immune system dysregulation and inflammatory processes in OUD and StUD. Future research should focus on further elucidating these unique aging processes, which may stem from substance-specific molecular signatures or from a combination of factors, such as environmental stressors, comorbidities, and lifestyle influences, that interact with substances use to accelerate biological aging. Understanding these interactions will be critical in developing targeted interventions to mitigate the health risks associated with premature aging in SUD populations.

Materials and Methods

Sample Characteristics and Brain Tissue Samples

Postmortem brain BA9 samples of 62 participants with SUD were obtained from The University of Texas Health Science Center at Houston (UTHealth) Brain Collection, in collaboration with the Harris County Institute of Forensic Science (HCIFS), under the approval of the Institutional Review Board, as described previously (8). For all subjects, informed consent was secured from the next-of-kin and demographic information, autopsy and toxicology reports, and medical and psychiatric notes were obtained if available (8). A structured psychological autopsy interview (30) was conducted with the donor's next-of-kin to obtain detailed information of mental health history, age of onset of drug use, types of substances used, drinking and smoking history, and any co-morbidities. An independent panel of three trained and licensed clinicians reviewed all available information to reach a consensus diagnosis for each subject, classifying them as having a SUD, from which subjects were then categorized into a specific SUD subgroup based on their primary diagnosis.

Four participants ($n = 4$) were excluded following FastQC quality control, and four additional participants ($n = 4$) were removed after being identified as consistent outliers based on Euclidean and Mahalanobis distances in PCA conducted on both cell type proportions and RNA counts. Hence, epigenetic age estimates and clustering analysis (section 2.2, below) were performed for 58 participants with SUD. The Shapiro–Wilk and Kolmogorov–Smirnov tests were used to assess the distribution of variables. Differences in categorical variables were examined using Chi-square tests, while continuous variables were evaluated with Student *t* tests for parametric distributions. Effect sizes were calculated using Cramér's V for Chi-square tests and the r statistic for Student *t* tests.

Epigenetic Clock Estimates and Clustering Analysis

Total DNA extraction and DNAm assays were performed, as described previously (8). Subsequently, DNAm data were processed using the *minfi* and *IlluminaHumanMethylationEPICanno.ilm10b4.hg19* packages (31). IDAT files were imported, and quality control steps included filtering samples with detection *p* values above 0.05 and removing probes with low bead counts. Functional normalization, combined with Noob normalization, was applied to correct for technical noise. Probes failing a detection p-value threshold of 0.01, those associated with SNPs, and those located on sex chromosomes were excluded. Beta values were obtained using the getBeta function, and M-values were obtained using the getM function from *minfi*.

Epigenetic aging was assessed using three clocks specifically designed for brain tissues: $\text{DNAmClock}_{\text{Cortical}}$, $\text{CerebralCortexClock}_{\text{common}}$, and PCBrainAge. $\text{DNAmClock}_{\text{Cortical}}$ was developed to improve the accuracy of age prediction, specifically in human cortex tissue, trained on chronological age using 347 CpG sites relevant to the cerebral cortex (32). The $\text{CerebralCortexClock}_{\text{common}}$ clock was designed to estimate DNAm age specifically for the cerebral cortex, trained using 201 age-associated CpG sites common across different non-cerebellar brain tissues (33). Finally, PCBrainAge was trained using a method of principal component projection on datasets that emphasize brain-specific DNAm patterns associated with Alzheimer's disease (34). $\text{DNAmClock}_{\text{Cortical}}$ and $\text{CerebralCortexClock}_{\text{common}}$ were computed using the *dnaMethyAge* package, while the PCBrainAge was computed using the *calcPCBrainAge* package.

In addition to the brain-specific clocks, we used the PC-Clock package to calculate PCHorvath1, PCHorvath2, PCHannum, PCPhenoAge, and PCGrimAge (35, 36). PCHorvath1 and PCHorvath2 are based on Horvath's original and revised multitissue clocks, respectively, while PCHannum is derived from the Hannum clock, initially trained on blood samples. PCPhenoAge and PCGrimAge are constructed from the PhenoAge and GrimAge clocks, often referred to as "second-generation" clocks, which predict phenotypic aging and mortality risk, respectively.

AA estimates were derived by calculating DNAm-predicted age and regressing this against chronological age, where positive residuals indicate faster-than-expected aging (i.e., AA), and negative residuals indicate slower-than-expected aging (12). To classify subjects into distinct clusters of aging trajectories based on the AA profiles from the three brain-specific clocks, PCA was applied to the standardized AA data to reduce dimensionality and capture the common aging signal across clocks. As PC1 explained 58% of the variance, participants were grouped based on PC1 scores, with positive scores indicating accelerated aging (AA+) and negative scores indicating non-accelerated aging (AA−) (Supplementary Figure S1). Although epigenetic aging is inherently a continuous process, this binary classification was adopted as a pragmatic strategy to enhance interpretability and statistical power in downstream transcriptomic analyses, particularly given the modest sample size. PCA-based grouping allowed us to aggregate the shared signal across partially non-converging clocks, minimizing the noise associated with individual clock variability.

Figure 3 shows the overlap of subjects identified as AA+ or AA− based on each clock, suggesting that although each clock captures distinct aspects of the aging process, there is considerable convergence in identifying individuals with AA in SUD. Correlations within all epigenetic variables, brain epigenetic variables, and chronological age were tested for the entire sample using Pearson tests with the *Hmisc* R package.

Next-generation RNA Sequencing and Differential Expression Analysis

RNA sequencing (RNA-seq) was carried out in BA9 bulk tissue from the same subjects as for DNAm, and data were trimmed for low-quality base pairs and adapter sequences using *trim_galore*, as described previously (36). Sequencing reads were mapped to the human genome build UCSC hg38 using STAR (37), and gene expression was quantified using featureCounts (38). Data was filtered and harmonized with reference gene signatures using curated gene expression profiles from the sigsBrain.rda file (https://rdrr.io/github/unawaz1996/brainyR/man/sigsBrain.html), based on publicly available brain single-cell RNA-seq data (39). The run.DTA function from the *dtangle* package (40) was used to estimate the relative proportions of each cell type, and composite neuronal proportions were calculated by combining excitatory and inhibitory neuron estimates.

Differential expression (DE) analysis was conducted using the R Bioconductor packages *edgeR* (41) and *limma* (42). Sample read counts were filtered to retain only expressed genes, and normalization was performed using the Trimmed Mean of M-values (TMM) method (*calcNormFactors* function in the *edgeR* package). The model matrix was fitted using *lmFit,* and empirical Bayes statistics (*eBayes*) were applied to identify DEGs. DE between AA+ and AA− was assessed for all the SUD samples ($n = 58$) and within each SUD subgroup based on their diagnosis (AUD = 13,

https://doi.org/10.61373/gp025a.0029

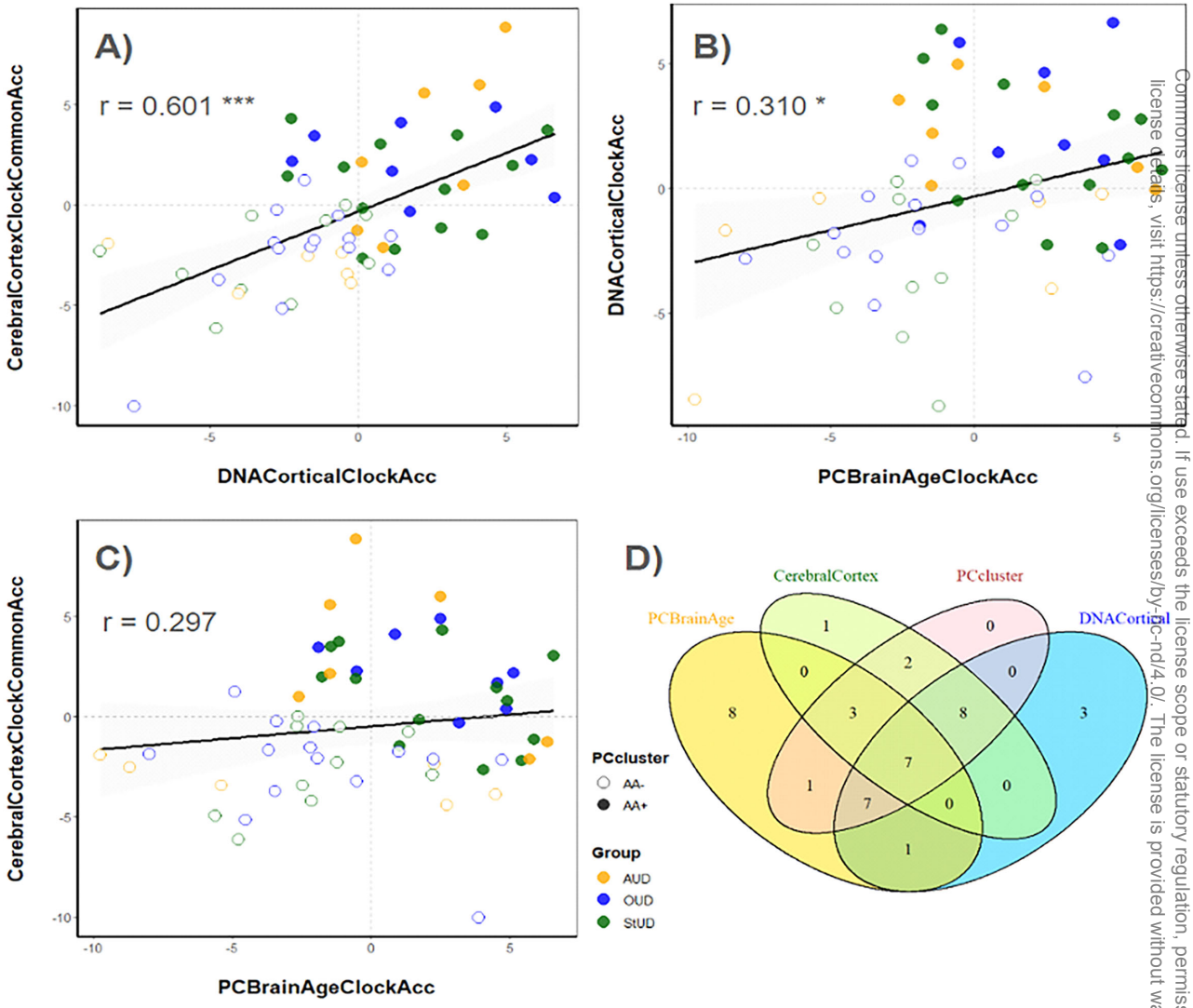

Figure 3. Pearson correlations and Venn diagram of overlaps between aging acceleration based on epigenetic clocks designed for brain tissue. (A–C) Scatter plots showing Pearson correlations between epigenetic aging acceleration measures derived from different brain-specific clocks. Each dot represents a participant, categorized based on their PC cluster classification: accelerated aging positive (AA+, filled dots) or accelerated aging negative (AA−, open circles). (D) Venn Diagram showing overlap of SUD subtypes: AUD (yellow), OUD (blue), and StUD (green). Correlation coefficients (*r*) are annotated for each pair of measures, with significance levels indicated ($^{*}p < .05$; $^{***}p < .001$). The shaded regions around the regression lines indicate 95% confidence intervals.

OUD = 16, StUD = 10). To minimize confounding effects, SUD subgroups were restricted to participants with a single primary SUD diagnosis, excluding those meeting the criteria for any additional SUD. The models were: ∼ *Accelerated Aging [AA+ vs. AA−] + Age [years] + Sex [male vs. female] + Batch [A vs. B] + postmortem interval [PMI in hours] + RNA integrity number [RIN] + tissue pH + smoking index [CpG methylation levels at cg05575921* (43, 44)*] + Astrocytes [proportion].* The proportion of astrocytes was included as a covariate because it accounted for a substantial portion of the variance (16%) in the variance partition analysis (Supplementary Table S1). Significant DEGs were identified based on a nominal *p*-value threshold of 0.01 and a fold change cutoff of 0.5. Results were visualized using EnhancedVolcano, highlighting significant DEGs across conditions. Finally, sensitivity analyses were performed, including individuals with an additional SUD (or secondary diagnosis).

Pathway Analyses

The DEGs were extracted and subjected to enrichment for GO: BP terms. Enrichment analysis was then conducted using the Database for Annotation, Visualization, and Integrated Discovery (DAVID, https://david.ncifcrf.gov) (45), enabling comparison of overlaps between enriched pathways. Significant pathways were identified with a nominal *p* value < 0.05.

Acknowledgments

We are grateful for the invaluable donations and participation from families, as well as for the generous collaboration of the medical examiners at the Harris County Institute of Forensic Sciences.

Data Availability

All data, including DNA methylation data, is available upon request.

Author Contributions

B.K.S. designed and conducted all data analyses and wrote the manuscript. L.S. oversaw processing of all biological samples, DNA methylation, and RNA-seq assays. T.B. contributed to data interpretation and manuscript writing. T.D.M. oversaw all psychological autopsy assessments. The manuscript has been read and approved by all authors. All authors take full responsibility for all data, figures, and text and approve the content and submission of the study. No related work is under consideration elsewhere. All authors state that all unprocessed data are available, and all figures provide accurate presentations of

the original data. Corresponding authors: G.R.F. for conceptualization of epigenetic clock analyses and C.W.B. for overall project conceptualization, postmortem brain collection, and project administration.

Funding Source

Support from RO1DA044859 and the John S. Dunn Foundation to C.W.B.

Author Disclosures

The corresponding author had full access to all the data in the study and had final responsibility for the decision to submit for publication. All authors have declared no conflict of interest.

References

1. World Health Organization. Global Status Report on Alcohol and Health. Geneva, Switzerland: World Health Organization; 2018, 469. Available from: https://play.google.com/store/books/details?id=qnOyDwAAQBAJ
2. Liu M, Savaskan N, Wang Z, Yang X, Sun Y. Epidemiological Characteristics and Related Risk Factors of the Older Population Aged Over 75 Years. Lausanne, Switzerland: Frontiers Media SA; 2023, 122. Available from: https://books.google.com/books/about/Epidemiological_characteristics_and_rela.html?hl=&id=7yyuEAAAQBAJ
3. Rusanen M, Kivipelto M, Quesenberry CP Jr, Zhou J, Whitmer RA. Heavy smoking in midlife and long-term risk of Alzheimer's disease and vascular dementia. Arch Intern Med. 2011;171(4):333–9. DOI: 10.1001/archinternmed.2010.393. PMID: 20975015
4. Horvath S. DNA methylation age of human tissues and cell types. Genome Biol. 2013;14(10):R115. DOI: 10.1186/gb-2013-14-10-r115. PMID: 24138928; PMCID: PMC4015143
5. Oblak L, van der Zaag J, Higgins-Chen AT, Levine ME, Boks MP. A systematic review of biological, social, and environmental factors associated with epigenetic clock acceleration. Ageing Res Rev. 2021;69:101348. DOI: 10.1016/j.arr.2021.101348. PMID: 33930583
6. Bernabeu E, McCartney DL, Gadd DA, Hillary RF, Lu AT, Murphy L, et al. Refining epigenetic prediction of chronological and biological age. Genome Med. 2023;15(1):12. DOI: 10.1186/s13073-023-01161-y. PMID: 36855161; PMCID: PMC9976489
7. Bachi K, Sierra S, Volkow ND, Goldstein RZ, Alia-Klein N. Is biological aging accelerated in drug addiction? Curr Opin Behav Sci. 2017;13:34–39. DOI: 10.1016/j.cobeha.2016.09.007. PMID: 27774503; PMCID: PMC5068223
8. Cabrera-Mendoza B, Stertz L, Najera K, Selvaraj S, Teixeira AL, Meyer TD, et al. Within subject cross-tissue analyses of epigenetic clocks in substance use disorder postmortem brain and blood. Am J Med Genet B Neuropsychiatr Genet. 2023;192(1-2):13–27. DOI: 10.1002/ajmg.b.32920. PMID: 36056652; PMCID: PMC9742183
9. Luo A, Jung J, Longley M, Rosoff DB, Charlet K, Muench C, et al. Epigenetic aging is accelerated in alcohol use disorder and regulated by genetic variation in APOL2. Neuropsychopharmacology. 2020;45(2):327–36. DOI: 10.1038/s41386-019-0500-y. PMID: 31466081; PMCID: PMC6901591
10. Zindler T, Frieling H, Fliedner L, Veer IM, Neyazi A, Awasthi S, et al. How alcohol makes the epigenetic clock tick faster and the clock reversing the effect of abstinence. Addict Biol. 2022;27(5):e13198. DOI: 10.1111/adb.13198. PMID: 36001430
11. Rosen AD, Robertson KD, Hlady RA, Muench C, Lee J, Philibert R, et al. DNA methylation age is accelerated in alcohol dependence. Transl Psychiatry. 2018;8(1):182. DOI: 10.1038/s41398-018-0233-4. PMID: 30185790; PMCID: PMC6125381
12. Zillich L, Cetin M, Hummel EM, Poisel E, Fries GR, Frank J, et al. Biological aging markers in blood and brain tissue indicate age acceleration in alcohol use disorder. Alcohol Clin Exp Res.2024;48(2):250–9 . DOI: 10.1111/acer.15241. PMID: 38276909; PMCID: PMC10922212
13. Martinez S, Jones JD. A pilot study examining the relationship between chronic heroin use and telomere length among individuals of African ancestry. Pharmacol Biochem Behav. 2023;231:173631. DOI: 10.1016/j.pbb.2023.173631. PMID: 37689117; PMCID: PMC10545475
14. Zhai T, Salmeron BJ, Gu H, Adinoff B, Stein EA, Yang Y. Functional connectivity of dorsolateral prefrontal cortex predicts cocaine relapse: implications for neuromodulation treatment. Brain Commun. 2021;3(2):fcab120. DOI: 10.1093/braincomms/fcab120. PMID: 34189458; PMCID: PMC8226190
15. la Torre A, Lo Vecchio F, Greco A. Epigenetic mechanisms of aging and aging-associated diseases. Cells. 2023;12(8):1163. DOI: 10.3390/cells12081163. PMID: 37190071; PMCID: PMC10136616
16. Carlson ME, Silva HS, Conboy IM. Aging of signal transduction pathways, and pathology. Exp Cell Res. 2008;314(9):1951–61. DOI: 10.1016/j.yexcr.2008.03.017. PMID: 18474281; PMCID: PMC2572856
17. Cox MF, Hascup ER, Bartke A, Hascup KN. Friend or Foe? Defining the role of glutamate in aging and Alzheimer's disease. Front Aging. 2022;3:929474. DOI: 10.3389/fragi.2022.929474. PMID: 35821835; PMCID: PMC9261322
18. Saul D, Kosinsky RL. Epigenetics of aging and aging-associated diseases. Int J Mol Sci. 2021;22(1):401. DOI: 10.3390/ijms22010401. PMID: 33401659; PMCID: PMC7794926
19. de la Monte SM, Jhaveri A, Maron BA, Wands JR. Nitric oxide synthase 3-mediated neurodegeneration after intracerebral gene delivery. J Neuropathol Exp Neurol. 2007;66(4):272–83. DOI: 10.1097/nen.0b013e318040cfa2. PMID: 17413318
20. Li J, Yue Z, Xiong W, Sun P, You K, Wang J. TXNIP overexpression suppresses proliferation and induces apoptosis in SMMC7221 cells through ROS generation and MAPK pathway activation. Oncol Rep. 2017;37(6):3369–76. DOI: 10.3892/or.2017.5577. PMID: 28440491
21. Bhatt NY, Kelley TW, Khramtsov VV, Wang Y, Lam GK, Clanton TL, et al. Macrophage-colony-stimulating factor-induced activation of extracellular-regulated kinase involves phosphatidylinositol 3-kinase and reactive oxygen species in human monocytes. J Immunol. 2002;169(11):6427–34. DOI: 10.4049/jimmunol.169.11.6427. PMID: 12444151
22. Dong F, Zhang X, Wold LE, Ren Q, Zhang Z, Ren J. Endothelin-1 enhances oxidative stress, cell proliferation and reduces apoptosis in human umbilical vein endothelial cells: role of ETB receptor, NADPH oxidase and caveolin-1. Br J Pharmacol. 2005;145(3):323–33. DOI: 10.1038/sj.bjp.0706193. PMID: 15765100; PMCID: PMC1576147
23. Liu Z, Morgan S, Ren J, Wang Q, Annis DS, Mosher DF, et al. Thrombospondin-1 (TSP1) contributes to the development of vascular inflammation by regulating monocytic cell motility in mouse models of abdominal aortic aneurysm. Circ Res. 2015;117(2):129–41. DOI: 10.1161/CIRCRESAHA.117.305262. PMID: 25940549; PMCID: PMC4490953
24. LeBlanc AJ, Kelm NQ. Thrombospondin-1, free radicals, and the coronary microcirculation: the aging conundrum. Antioxid Redox Signal. 2017;27(12):785–801. DOI: 10.1089/ars.2017.7292. PMID: 28762749; PMCID: PMC5647494
25. Dunaway LS, Pollock JS. HDAC1: an environmental sensor regulating endothelial function. Cardiovasc Res. 2022;118(8):1885–903. DOI: 10.1093/cvr/cvab198. PMID: 34264338; PMCID: PMC9239577
26. Jonatan D, Spence JR, Method AM, Kofron M, Sinagoga K, Haataja L, et al. Sox17 regulates insulin secretion in the normal and pathologic mouse β cell. PLoS One. 2014;9(8):e104675. DOI: 10.1371/journal.pone.0104675. PMID: 25144761; PMCID: PMC4140688
27. Lv J, Yi Y, Qi Y, Yan C, Jin W, Meng L, et al. Mitochondrial homeostasis regulates definitive endoderm differentiation of human pluripotent stem cells. Cell Death Discov. 2022;8(1):69. DOI: 10.1038/s41420-022-00867-z. PMID: 35177589; PMCID: PMC8854419
28. Narendra S, Klengel C, Hamzeh B, Patel D, Otten J, Lardenoije R, et al. Genome-wide transcriptomics of the amygdala reveals similar oligodendrocyte-related responses to acute and chronic alcohol drinking in female mice. Transl Psychiatry. 2022;12(1):476. DOI: 10.1038/s41398-022-02231-2. PMID: 36371333; PMCID: PMC9653459
29. Lin SM, Frank DB. SOX17 at the intersection of sex, transcription, and metabolism in pulmonary hypertension. Am J Respir Crit Care Med. 2023;207(8):971–2. DOI: 10.1164/rccm.202302-0284ED. PMID: 36927296; PMCID: PMC10112455
30. Meyer TD, Godfrey CJ, Walss-Bass C. The UT health psychological autopsy interview schedule (UTH-PAIS) – description and reliability of diagnoses and transdiagnostic personality measures. J Psychiatr Res. 2022;156:221–7. DOI: 10.1016/j.jpsychires.2022.10.014. PMID: 36270060
31. Aryee MJ, Jaffe AE, Corrada-Bravo H, Ladd-Acosta C, Feinberg AP, Hansen KD, et al. Minfi: a flexible and comprehensive bioconductor package for the analysis of Infinium DNA methylation microarrays. Bioinformatics. 2014;30(10):1363–9. DOI: 10.1093/bioinformatics/btu049. PMID: 24478339; PMCID: PMC4016708
32. Shireby GL, Davies JP, Francis PT, Burrage J, Walker EM, Neilson GWA, et al. Recalibrating the epigenetic clock: implications for assessing biological age in the human cortex. Brain. 2020;143(12):3763–75. DOI: 10.1093/brain/awaa334. PMID: 33300551; PMCID: PMC7805794
33. Wang Y, Grant OA, Zhai X, Mcdonald-Maier KD, Schalkwyk LC. Insights into ageing rates comparison across tissues from recalibrating cerebellum DNA methylation clock. Geroscience. 2024;46(1):39–56. DOI: 10.1007/s11357-023-00871-w. PMID: 37597113; PMCID: PMC10828477
34. Thrush K, Markov Y, Higgins-Chen A, Morgan L. PCBrainAge: a brain-specific AD-associated DNA methylation clock. Alzheimers Dement. 2022;18:e069230. Available from: https://onlinelibrary.wiley.com/doi/abs/10.1002/alz.069230
35. Du P, Zhang X, Huang CC, Jafari N, Kibbe WA, Hou L, et al. Comparison of beta-value and M-value methods for quantifying methylation levels by microarray analysis. BMC Bioinformatics. 2010;11:587. DOI: 10.1186/1471-2105-11-587. PMID: 21118553; PMCID: PMC3012676

36. Mendez EF, Wei H, Hu R, Stertz L, Fries GR, Wu X, et al. Angiogenic gene networks are dysregulated in opioid use disorder: evidence from multi-omics and imaging of postmortem human brain. Mol Psychiatry. 2021;26(12):7803–12. DOI: 10.1038/s41380-021-01259-y. PMID: 34385598; PMCID: PMC8837724
37. Dobin A, Gingeras TR. Optimizing RNA-seq mapping with STAR. Methods Mol Biol. 2016;1415:245–62. DOI: 10.1007/978-1-4939-3572-7_13. PMID: 27115637
38. Fdez-Riverola F, Rocha M, Mohamad MS, Caraiman S, Gil-González AB. Practical Applications of Computational Biology and Bioinformatics, 16th International Conference (PACBB 2022). L'Aquila, Italy: Springer Nature; 2022, 122. Available from: https://play.google.com/store/books/details?id=riuWEAAAQBAJ
39. Sutton GJ, Poppe D, Simmons RK, Walsh K, Nawaz U, Lister R, et al. Comprehensive evaluation of deconvolution methods for human brain gene expression. Nat Commun. 2022;13(1):1358. DOI: 10.1038/s41467-022-28655-4. PMID: 35292647; PMCID: PMC8924248
40. Hunt GJ, Freytag S, Bahlo M, Gagnon-Bartsch JA. dtangle: accurate and robust cell type deconvolution. Bioinformatics. 2019;35(12):2093–9. DOI: 10.1093/bioinformatics/bty926. PMID: 30407492
41. Chen Y, Chen L, Lun ATL, Baldoni PL, Smyth GK. edgeR v4: powerful differential analysis of sequencing data with expanded functionality and improved support for small counts and larger datasets. bioRxiv. 2024. DOI: 10.1101/2024.01.21.576131
42. Ritchie ME, Phipson B, Wu D, Hu Y, Law CW, Shi W, et al. limma powers differential expression analyses for RNA-sequencing and microarray studies. Nucleic Acids Res. 2015;43(7):e47. DOI: 10.1093/nar/gkv007. PMID: 25605792; PMCID: PMC4402510
43. Gadd DA, Stevenson AJ, Hillary RF, McCartney DL, Wrobel N, McCafferty S, et al. Epigenetic predictors of lifestyle traits applied to the blood and brain. Brain Commun. 2021;3(2):fcab082. DOI: 10.1093/braincomms/fcab082. PMID: 34041477; PMCID: PMC8134833
44. Zillich L, Poisel E, Streit F, Frank J, Fries GR, Foo JC, et al. Epigenetic signatures of smoking in five brain regions. J Pers Med. 2022;12(4):566. DOI: 10.3390/jpm12040566. PMID: 35455681; PMCID: PMC9029407
45. Sherman BT, Panzade G, Imamichi T, Chang W. DAVID ortholog: an integrative tool to enhance functional analysis through orthologs. Bioinformatics. 2024;40(10):btae615. DOI: 10.1093/bioinformatics/btae615. PMID: 39412445; PMCID: PMC11520416